

# THE SPIRAL FACETS

## *A Unified Framework for the Analysis and Description of 3D Facial Mesh Surfaces*

Naoufel Werghi, Harish Bhaskar

*Dept. of Computer Engineering, Khalifa University, Sharjah Campus, Sharjah, U.A.E.*

Youssef Meguebli, Haykel Boukadida

*School of Science and Techniques, University of Tunis, Tunis, Tunisia*

**Keywords:** 3D Face descriptors, Spiral facets, Feature localization, Geodesic curves, 3D Face orientation.

**Abstract:** In this paper, we describe a framework for encoding 3D facial triangular mesh surface. We derive shape information from the triangular mesh surface by exploiting specific arrangements of facets in the model. We describe the foundations of the framework and adapt the framework for several original applications including: face landmark detection, frontal face extraction, face orientation and facial surface representation. We validate the framework through experimentation with raw 3D face mesh surfaces and demonstrate that the model allows simpler implementation, more compact representation and encompasses rich shape information that can be usefully deployed both locally and globally across the face in comparison to other standard representations.

## 1 INTRODUCTION

Face recognition is a central problem in biometric authentication, with applications including visual surveillance and security. However, 2D face recognition systems are complicated by sensitivity to illumination conditions and pose variation. A popular alternative to such 2D image-based systems is the use of 3D face images whose richness and completeness is often exploited to contribute in solving the inherent limitations of 2D systems. However, there is a growing need to faithfully encode raw 3D facial mesh surface into a simple, structured and compact facial representation.

There exist competing approaches to model 3D facial mesh surfaces. 3D shape can be represented independent of the co-ordinate system using the object-centric representations. Such representations have invited much attention in recent years due to their invariance to geometric transformations and their potential to produce an reliable metric for facial shape comparison.

In this paper, we propose a topological framework for encoding 3D facial mesh surface that is concise (encompasses dimensionality reduction, as a means of improving the efficiency, or allowing the data compression) and computationally efficient. We denote this representation as the "spiral facets" and show

how this representation can be neatly adapted to address several applications including but not restricted to: facial landmarks detection, frontal face extraction, face shape description and face pose computation.

## 2 RELATED WORK

In the context of 3D face recognition, we can categorize the face shape representations into three classes, namely: Local features representation, global feature representation and hybrid representations.

Local feature representation methods employ features derived from local face surface (at a limited neighborhood). These attributes typically include curvature measures (Moreno et al.,2006), and point signatures (Chua et al.,2000). The derivation of local features is performed with differential geometry techniques that are intrinsically vulnerable to scaling and data deficiencies (e.g., non-uniform resolution, presence of noise).

In contrast to the local representation, in global representation, the facial features are derived from the whole 3D face data. Wu (Wu et al.,2003) used vertical and horizontal profiles of faces and Xu (Xu et al.,2008) derived invariant curve and surface moments from 3D face data. In these methods, match-

ing is performed by evaluating the similarity between these entities. Other methods (Irfanoglu et al.,2004; Lu and Jain,2005) superimpose the whole query 3D facial image with the stored instances in the database, and then evaluate the degree of overlapping to decide whether or not they match. These approaches are limited by their high computational cost. In (Lee et al.,2003; Xu et al.,2004b) authors, extend the eigenfaces paradigm developed in 2D face recognition to the 3D case. This paradigm operates on a range or depth image in which the pixel intensity represents the 'z' coordinate. However, these methods have inherited some of the shortcomings of 2D face identification, particularly with regard to the face pose, self-occlusion and scaling. Other representations have been developed based on geodesic entities (Bronstein et al.,2003; Berretti et al.,2006; Samir et al., 2009), these approaches aimed also to address face shape deformation. So did (Kakadiaris, 2007) with their deformable face model.

Finally, hybrid representation combines local and global facial features. These methods were motivated by psychological findings asserting that humans equally rely on both local and global visual information. Pan (Pan et al.,2003) augmented the eigenface paradigm with face profile. Xu (Xu et al.,2004a) developed a face representation defined by a measure of the similarity between the 3D face image and a 3D face template, and local shape variation around local facial landmarks (e.g., eyes and nose). Al-Osaimi (Mian et al.,2007) employed a 2D histogram that encompasses rank-0 tensor fields extracted at local points of the facial surface and from the whole face depth map data.

### 3 CONTRIBUTIONS & STRUCTURE

The framework described in this paper, extracts ordered structured patterns from 3D triangular mesh surface for a simple representation of facial surfaces. We acknowledge that there are a number of representations of 3D facial surfaces in the literature and therefore, we list a set of 4 main characteristics of our proposed "spiral facets" representation that will distinguish it from other close face shape representation (Berretti et al., 2006; Samir et al., 2009). These characteristics include: a) simplicity and compactness: the spiral facet representation is a single data structure, b) generalization: the facet spiral is a generalized representation of other popular 3D facial surface representations and it is possible that we can derive for example, the approximate geodesic rings structure

from the spiral facet, c) processing efficiency: our representation also does not require any form of mesh pre-processing, whereas in most other method mesh regularization is often required and finally, d) computational complexity: our method is computationally more efficient. As we will explained in the end of Section 4, we infer a complexity of  $O(n)$  in comparison to  $O(n \log(n))$  in (Berretti et al., 2006; Samir et al., 2009) which also requires a mesh regularization of complexity  $O(n)$ .

The other main novelty of the proposed framework is in the adaptability of the framework for several original applications including: a) nose tip localization, b) frontal face extraction, c) 3D face shape modeling d) 3D face pose computation and e) nose profile identification.

We begin by describing our framework of 3D facial surface representation in Section 4. We then elaborate different applications of the proposed framework in section 5 and conduct systematic experiments on varied datasets for nose tip localization 5.1, 3D frontal face extraction 5.2, face shape description 5.3, 3D face pose computation 5.4 and nose profile identification 5.5. In Section 6 we present concluding remarks and directions of future work.

## 4 THE SPIRAL FACETS FRAMEWORK

In our framework, we derive a 3D facial surface representation by constructing novel structured and ordered patterns in a 3D face triangular mesh surface. The triangular mesh surface representation though is simple, lacks an intrinsic ordered structure that allows the facets in the mesh to be browsed systematically. Consequently, storing the facets in the facet array is usually arbitrary and does not follow any particular arrangement. Therefore processing and analyzing triangular mesh surfaces are more complex compared with other intrinsically ordered shape modalities such as range images. According to our framework, we construct patterns exploiting topological properties of a triangular mesh surface. These patterns include concentric rings of facets that can also be arranged in a spiral-wise fashion. Our framework has been inspired from the observation of the arrangement of triangular facets lying on closed contour of edges (Figure 1.a). From this, we can categorize the facets into two groups: 1) facets having an edge on that contour that seem to point outside the area delimited by the contour (e.g.  $f_{out_1}$  and  $f_{out_2}$  in Figure 1.a). And 2) facets having a vertex on the contour that point inside the contour's area. The facets in the second group

have an effect of filling gaps between facets in the first group. We call these two groups of facets as *Fout* and *Fgap* facets and together, they form a kind of ring structure. Using this ring facets we can derive a new group of *Fout* facets that are one-to-one adjacent with the *Fgap* facets of the previous ring, that will in-turn form the basis of the subsequent rings (Figure 1.b). We iterate this process to obtain a group of concentric rings. When the initial contour is composed of the edges of a given triangular facet, the rings will be centered at that particular facet (Figure 1.c). Moreover, by imposing the last facet in the current ring to be connected to the first facet in the subsequent ring, we obtain a sequence of facets arranged on a spiral-wise fashion, i.e. sequence of facets starting at the root facet and following a spiral path on the facial surface. We dubbed this arrangement "the spiral facet". (Figure 1.d). We also note that from the root triangle 3 different spiral facets can be generated depending on the chosen facet among the three facets adjacent to the root facet.

The algorithm for constructing a facet spiral starting at a given facet  $t$  is as follows:

**Algorithm GetSpiralFacets.**

Rings = [  $t$  ], FoutFacets  $\leftarrow$  facets adjacent to  $t$

**For**  $i=1$ : Number of rings

GapFacets  $\leftarrow$  FillGap(FoutFacets)

Ring  $\leftarrow$  FoutFacets + GapFacets

Append Ring to Rings

NewFoutFacets  $\leftarrow$  GetFoutFacest

(GapFacets,FoutFacets)

FoutFacets  $\leftarrow$  NewFoutFacets

**End For**

The algorithm *GetSpiralFacets* has computational complexity of  $O(n)$  where  $n$  is the number of facets in the facet spiral.

One of the main interesting characteristics of the spiral facets representation is that facets at a given ring are approximately at the same geodesic distance from the root facet. The geodesic distance can be approximated to  $RingNumber \times L$ , where *RingNumber* is the ring's number in the facet spiral, and  $L$  is the average length of the triangle's edge. Therefore, it is possible to use the spiral facets as a low cost alternative for computing an approximation of iso-geodesic contours on the facial surface, compared to the standard  $O(n \log(n))$  Dijkstra algorithm (Cormen et al., 2001) (employed in (Samir et al., 2009)) and the  $O(n \log(n))$  fast marching method (Sethian and Kimmel, 1998) (used in (Berretti et al., 2006)). We compute the geodesic path using the spiral facets in two distinctive stages (Figure 1.e). In the first step, the spiral facets are expanded from a source facet until

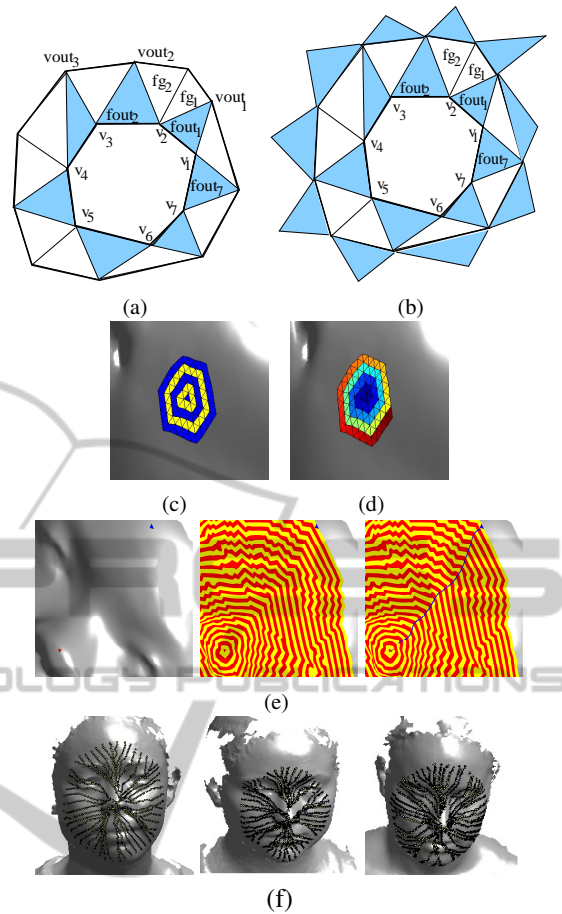


Figure 1: a): *Fout* facets (dark) on the contour  $E_7$  :  $(v_1, v_2, \dots, v_7)$ . The *Fgap* facets (clear) bridge the gap between pairs of consecutive *Fout* facets. b): Extraction of the new *Fout* facets. Notice that the new *Fout* facets are one-to-one adjacent to the *Fgap* facets. c): An examples of facet spiral and its concentric rings. d): The same facet spiral where the facets are arranged spiral-wise. e): Example of a geodesic path computation: The facet spiral is expanded from a source facet on the nose tip until the the destination facet is reached, then the geodesic path is extracted by tracing back the source facet. f): examples of geodesic paths between the nose tip and facets on a periphery ring of a facet spiral.

the destination facet is reached (i.e., found in the last ring). In the second step, the rings are browsed backwards, starting from the destination facet, and reiterated looking for the nearest connected facet in the previous ring until the source facet is reached. Since the algorithm *GetSpiralFacet* intrinsically computes the connectivity between facets in adjacent rings, the second stage has a complexity of  $O(RingNumber)$ . (Figure 1.f) depicts facets on the geodesic paths between the nose tip and facets located at a given ring of the facet spiral.

## 5 APPLICATIONS

In this section of the paper, we exhibit the generality of the spiral facets framework by adapting it for several 3D face applications. One of the critical steps towards face recognition is the localization of features. In the initial attempt to localize 3D facial features using the "spiral facets" representation, we first present the nose tip detection application in Section 5.1. We substantially elaborate on this part since the rest of the applications depends on it. Next, we describe the algorithm to extract the frontal face from the raw 3D face scan by propagating rings starting from the detected nose tip in Section 5.2. Face shape description and pose identification are also important components particularly to model based matching of 3D faces. In Sections 5.3,5.4 we explore an approach for face shape description and face pose computation using the spiral facets framework. Finally, we also exploit the geodesic properties of the spiral facets to extract the nose profile from 3D face scans in Section 5.5.

### 5.1 Nose Tip Detection

Face landmarks detection is critical to face recognition and nose tip detection in particular has a capital role due to its center position and saliency. A majority of 3D face analysis techniques are anchored to detecting the nose tip. The problem of nose tip detection has been approached using heuristic rules-based methods (Colbry et al., 2005; Heseltine et al., 2008). Such methods requires a restricted face pose. This issue was addressed to some extent by shape descriptors-based methods (Segundo et al., 2007; Wang et al., 2008) that are specifically invariance to geometric transformation. However, the presence of noise has often affected the reliability of such systems. Statistical methods (Ruiz and Illingworth,2008; Romero and Pears, 2009) employed a landmarks model, obtained via training. This model is registered to the face data in order to get an approximate landmark locations, which are further refined in an iterative manner. This method inherits the problems of model registration; such as the need of prior pose information. Apart of (Xu et al., 2006) most approaches that dealt with face landmarks detection treated a pre-processed data, in which the 3D face surface has been cropped and smoothed. The method in (Xu et al., 2006) uses a hierarchical filtering scheme employing shape descriptors and a local nose tip shape model. The method is robust, but, revealed cases of false detection for some instance where clothing deformation matches the nose tip statistical model.

We propose an application of the 3D spiral facets for nose tip detection from raw 3D triangular mesh facial surfaces. Our method is inspired from the observation that the regions around some facial landmarks are characterized by low mesh quality. These result from gaps (in the nostrils) and reflection effects (at the eyes) (see Figure 2.a). To measure and assess the quality of the mesh surface, we present an original framework using which we extract a group of candidate triangular facets. In the second stage of our algorithm, we find the single facet that corresponds to the nose tip from the group of candidate triangle facets using a series of filtering steps.

#### 5.1.1 Assessing the Regularity of the Mesh Tessellation

The term mesh quality is context driven and tightly linked to the subsequent use of the constructed mesh (Frey and Borouchaki, 1999), therefore there is no standard framework for assessing the quality of triangular mesh surface for raw 3D facial surface scan.

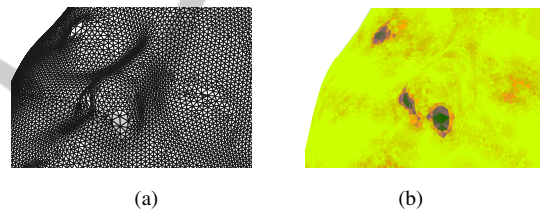


Figure 2: a): A sample triangular mesh facial surface. Notice the mesh irregularities at the nostrils, and the the eyes areas. b): Computation of the error  $\Delta_3$  at each facet. Dark areas correspond to a large error.

Our proposed technique measures to what extent a triangular mesh is close to an ideal mesh composed of equal-sized equilateral triangles at a given neighborhood. In such mesh, we can show easily that the number of triangles across the concentric rings that from the facet spiral follow arithmetic progression:

$$nrt(n+1) = nrt(n) + 12 \quad (1)$$

where  $nrt(n)$  and  $nrt(n+1)$  are the number of triangles in the ring  $n$  and  $n+1$  respectively. Therefore, the sequence  $\hat{\eta}_n$  in an ideal mesh, starting at a root facet, is  $[12, 24, 36, \dots, 12n]$ . This condition will not be satisfied at surface areas where the uniformity of the mesh tessellation is corrupted. Based on this, we propose the following local criterion for evaluating the mesh tessellation uniformity.

$$\Delta_n = \frac{\|\eta_n - \hat{\eta}_n\|}{\|\hat{\eta}_n\|}, \quad (2)$$

where  $\eta_n$  (respectively  $\hat{\eta}_n$ ) is the sequence representing the number of triangles across a group of  $n$  concentric rings in an arbitrary mesh (respectively an ideal mesh). Figure 2.b depicts  $\Delta_3$  computed at each facet of a sample 3D raw facial data.

### 5.1.2 Cascading filters

After computing the error  $\Delta_n$  (Figure 3.b), we retain those facets having a  $\Delta_n$  above a certain threshold. The group of facets extracted from this level of filtering (dubbed Group1), contains a majority of facets in the neighborhood of the nostrils and eyes and also other facets spread mostly across the ears, clothes and the periphery areas in the raw mesh surface (as in Figure 3.c). In the second level of our cascaded filtering implementation, we apply prior information derived from the topological characteristics of the raw face scan to extract the central facets corresponding to a potential landmark. As Figure 3.a shows, the face scan is composed of several fragmented manifold pieces which includes the face, parts of the hair, neck, and upper torso. We initialize a two-phase filter where in the first phase, facets from Group1 generating more than 18 rings are selected. By doing this, we capture facets located within the vicinity of the central face, and naturally discard those which are located at the surface periphery or at small surface fragments. We set the threshold to 18 as it is about half the maximum number of rings in a typical facial surface. In the subsequent phase, we select from the obtained facets those scoring the 10 highest number of rings (Figure 3.d). To these facets we add those located at their neighborhoods (by expanding 4 rings-facet spiral around each one of them). We called the so obtained group of facets, Group 2 facets.

In the third level, we employ a model-based matching method based on the standard Geometric Histogram (GH) local shape descriptor (Ashbrook et al., 1998). The GH is a 2D accumulator that describes a pairwise relationship between a central facet and each of its surrounding facets within a given neighborhood. This relationship in the form of the angles ( $\alpha$ ) between the central facet normals and all the other facets' normals, and the range of perpendicular algebraic distances ( $\rho$ ) from the plane in which the central facet lies to all the other facets in the neighborhood. These measurements are entered in the discrete angle\_distance 2D accumulator, thus obtaining a kind of distribution that characterizes the relationship between the root facet and its neighbors. The neighborhood is constructed by generating a six-rings spiral facets around a central facet. At this level, the GH of each candidate facet is matched with the statistical model of GH of the nose tip neighborhood.

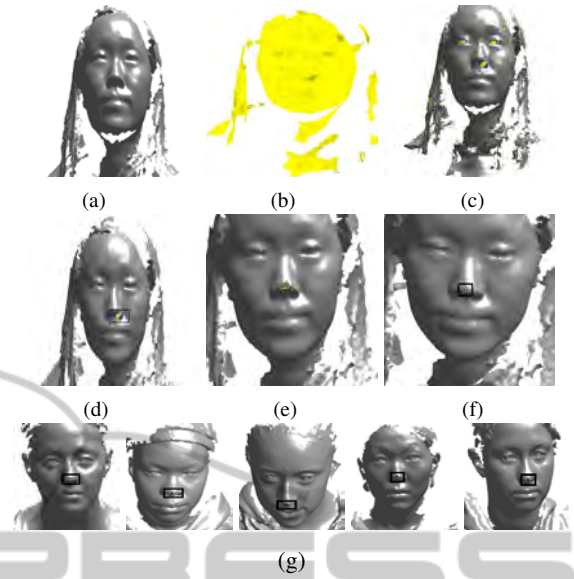


Figure 3: Nose tip detection stages a: raw 3D face mesh surface. b: computation of the mesh quality criterion  $\Delta_n$ . c: Selection of the facets scoring a  $\Delta_n$  above a certain threshold. d: Elimination of the facets at the periphery areas and selection of the most central facets. e: Detection of candidate facets via Geometric Histogram matching. f: selection of the nose tip facet. g: Detected nose tips on some face samples.

This model is obtained from 100 face data samples, whereby we averaged the 100 GHs derived from their corresponding nose tip neighborhoods.

The matching criterion used to evaluate the closeness of two GHs  $h_i$  and  $h_j$  is the Bhattacharyya distance:

$$D_{Bhattacharyya}^{ij} = \sum_{\alpha, \rho} \sqrt{h_i(\alpha, \rho)} \sqrt{h_j(\alpha, \rho)}. \quad (3)$$

Since the nose tip can be located as an area rather than a single point, and the matching is performed using an average model, we select the facets having a matching score at a given distance from the maximum. This set of facets, called Group 3, is defined by:

$$\mathcal{N} = \{t \mid \text{Max}_D - 5\sigma \leq D_{Bhattacharyya}(GH_t, GH) \leq \text{Max}_D\} \quad (4)$$

where sigma is the variance of Bhattacharyya distances between the GHs samples used for computing the mean GH model. Figure 3.e depicts an instance of this set. In the final level of our cascaded filtering implementation, we further refine the location of the nose tip by computing for each facet in Group 3, the rank-2 tensor field (Mian et al., 2007)

$$T = \sum_{i=1}^n \frac{a_i \vec{r}_i \vec{r}_i^T}{A \|\vec{r}_i\|^2} \quad (5)$$

where  $n$  is the number of facets in the facet's neighborhood.  $a_i$  is the area of the  $i$ th facet,  $\vec{r}_i$  is a vector from its center to central facet's center and  $A$  is the total neighbourhood's area.  $T$  represents the covariance of  $\vec{r}$  and encodes the local neighborhood variation which is reflected in its three eigenvalues. So in this level we select the facet having the largest eigenvalue as the one corresponding to the nose tip. Figure 3.(f,g) shows nose tips detected on some face samples.

## 5.2 Frontal Face Extraction

Using the same framework for assessing mesh quality, and exploiting the knowledge of the nose tip area, we present an extension to extract the frontal face area from the raw unprocessed 3D facial data. A popular technique to extract frontal faces discussed in the literature is using a cropping sphere centered at the nose tip (e.g. in (F. R. et al., 2008; Nair and Cavallo, 2009)). However such a technique is sensitive to scale variance. An alternative approach discussed in (R. Niese et al., 2007) uses 3D point clustering based on texture information. This method requires the texture map to be available, and is unstable for head orientations greater than  $\pm 45^\circ$ .

In our approach, we exploit the spiral facets to develop an intrinsically scale-invariant method for frontal face extraction. Its implementation is as follows: For each facet  $t$  within a 5-ring size nose tip neighborhood, we generate a set of facets  $\mathcal{R}(t)$  using the *GetFacetSpiral* algorithm initialized at  $t$  and with the stop condition set to 'Rings reaches a border of the surface'. Following which, we merge all the sets  $\mathcal{R}(t)$  into a single set  $\mathcal{F}$  using:

$$\mathcal{F} = \uplus_{t \in \mathcal{N}} \mathcal{R}(t) \quad (6)$$

where  $\uplus$  is the exclusive union. This procedure ensures a maximum coverage of the central face area.

An illustration of the frontal face extraction process is shown in Figure 4.

## 5.3 Face Shape Description

We discuss the 3rd application of the spiral facets framework in the form of the face shape description. From the spiral facets we derive a discrete 3D curve represented by a sequence of points  $P_1, \dots, P_n$  where each point is the center of a triangle facet. This curve is invariant to translation and rotation. The curve exhibits some irregularity inherited from the raw triangular mesh. Rather than performing a costly mesh regularization preprocessing stage, we simply apply basic spatial smoothing to the points followed by a 3D

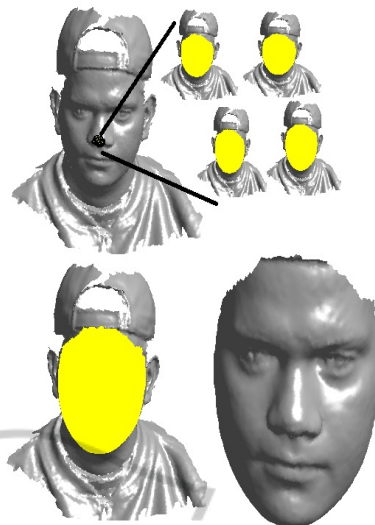


Figure 4: Extraction of the frontal face area: from the each facet in the nose tip neighborhood we propagate rings until a border is reached. Then we merge the obtained sets to get the frontal face area.

Chord Length parametrization and cubic spline interpolation (Piegl and Tiller, 2006). The parametrization is performed as follows:

$$t_0 = 0 \quad t_k = \frac{1}{L} \left( \sum_{i=1}^k |P_i - P_{i-1}| \right) \quad t_n = 1; \quad (7)$$

Since the chord length parametrization in an approximation of the area-length parametrization, the parameter space of the spiral curve generates a sequence of 3D points at nearly uniform intervals. Figure 5.a shows a portion of 3D spiral curve starting at the nose tip. Figure 5.b shows an instance of 3D spiral curve spanning the whole face superimposed on the original surface. This spiral 3D curve encapsulates the facial shape variation at a both local and global scale. Moreover, since the 3D spiral curve is attached to the facial surface, it can be augmented to the normal to the face surface at each of points. We presume that our facial representation spiral facets is the only model that encode such facial shape variation into a single mono-dimensional structure. In the same vein, we construct a 3D closed curve from each ring in the spiral facets. We obtain a group of concentric curves  $C_k, k = 1..N$  centered at the nose tip. We can easily control the density of these curves by a simple subsampling as illustrated in Figure 5.(c). The  $C_k$  curves inherit from the spiral facet rings the iso-geodesic property. Therefore they can be used as low-cost alternative of the iso-geodesic closed curves employed in (Samir et al., 2009), which do also require a mesh regularization.

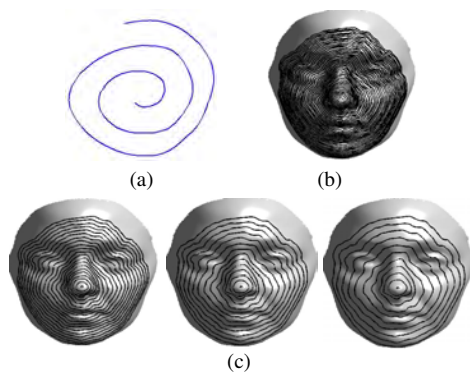


Figure 5: a): A piece of 3D spiral curve emanating from the nose tip. b): The full spiral curve superimposed on the facial surface. Facial closed-curves at decreasing sampling rate.

#### 5.4 Face Pose Computation

The computation of the face pose is a critical step to model based localization and recognition tasks. In this section, we brief on the details of how our framework is adapted to approximate the face pose of a 3D facial surface. By face pose, we refer to the coordinate system  $(O, \vec{u}, \vec{v}, \vec{w})$ , attached to the face, in which the origin is the nose tip, and the axis are the gaze direction, the normal to the face symmetry plane, and the view up direction. In order to determine the face pose: we begin by grouping all the points that form the discrete curves  $C_k$  determined in the previous section, and simply compute their principal axes via the standard PCA analysis. Since the curves  $C_k$  inherit the symmetry property of the facet with respect to face's symmetry plane, it is expected that the PCA method will produce axis that match the face pose to a reasonably good extent. In Figure 6.a we depict some examples of face pose axis plotted on the raw facial scans. From the face pose, we also derive the face symmetry plane, having as normal the vector  $\vec{v}$  and including the nose tip. Some examples of the symmetry plane are illustrated in Figure 6(2nd row). We assess the pose estimation methods in two ways, 1) by aligning pairs of different face scans of the same individuals using their estimated poses and 2) by comparing the symmetry plane computed by our method with symmetry plane derived from ground truth data. The first experiment was conducted with a group of faces comprising instances of raw facial scan in neutral expression and their sad expression counterpart. The facial surface in this last group are cropped. Figure 6 (3rd and 4th row) shows some aligned instances. It is clearly observable that alignments exhibit an acceptable accuracy, and thus can be used for a suitable initialization for the iterative registration algorithms such as the it-

erative closest point method (ICP).



Figure 6: Computation of the face pose (1st row) and deduction of the face symmetry plane for some face samples (2nd row). 3rd and 4th rows: Alignment of cropped instances of faces exhibiting sad facial expression to their counterparts raw images in a neutral expressions.

In the second method of assessment, we consider symmetry plane estimation error as the angle between the two normals of the estimated and the actual planes. We computed the estimation error for a group of 200 3D face instances (100 neutrals and 100 sads) and have found a standard deviation error of 2 degree for a mean error of 0.03 degree, and a maximum error of 4 degree.

In addition, we also assess the stability of the face pose estimate against increasing number of rings that define the faceprint. Here, we consider 100 sample images, 56 female and 44 male subjects at neutral positions. For each sample, we compute the face orientation for increasing percentages of the number rings starting 10% to 90% in steps of 20%. In Figure 7, we illustrate sample results of the aforementioned experiment. Rows 1 to 3 depict the face orientation with 30%, 50% and 70% of the maximum number rings and rows 4 to 6 shows the corresponding symmetry planes for different face samples (columns). As we can visually notice, the face pose stabilizes nearly at 50% of the maximum number of rings that is required to describe the facial surface.

To further probe the issue of the stability of face pose, we construct histograms of the percentage of number of face images that exhibit stable face orientation against increasing percentage of the number of rings on distinguished male and female subjects as in Figure 8. We measure stability in face pose as the difference in the angular distance between consecutive face pose estimates with increasing rings being lesser than a predefined threshold (which is 0.15 in

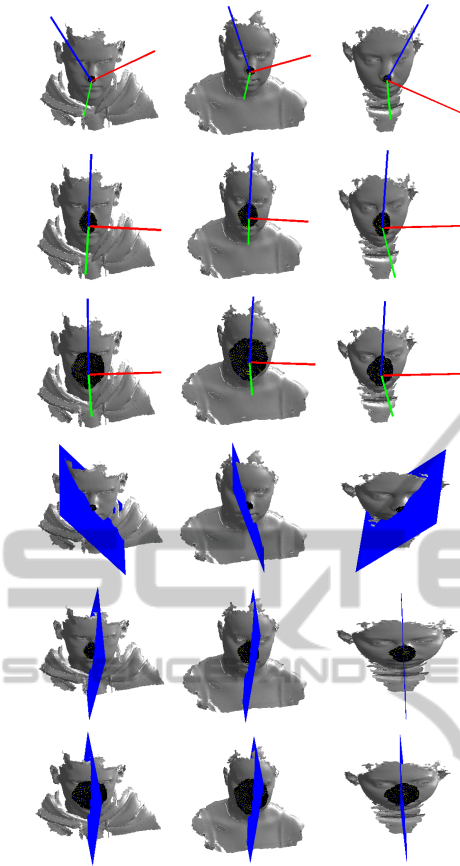


Figure 7: Stability of the face pose (1-3 columns) and the corresponding face symmetry plane (4-6 columns) with increasing number of rings (20% rise) on different face samples (columns).

our case). It is clear that over 92% of samples need just 70% of the maximum rings to produce stable face orientations and nearly 60% of samples need 50% of the maximum rings to produce stable face pose estimates.

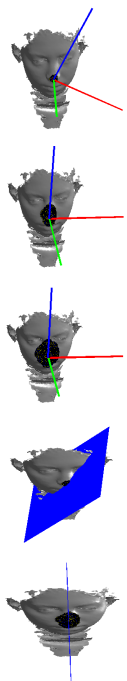


Figure 8: Percentage of face with stabilized face orientation (y-axis) versus the percentage increase in the number of rings across male (blue) and female (yellow) samples.

### 5.5 Nose Profile Identification

As the final application of the spiral facets framework, we describe the problem of nose profile identification. We define the nose profile as a curve that joins the nose bridge with the nose tip across the face plane of symmetry. This curve follows the path of high curvature along the nose, which nearly coincides with shortest path between these two points. We extend our framework based on geodesic paths as described at the end of 4 to identify the nose profile. In effect, at it is shown in Figure 1.f, geodesic paths that join neighboring facets, in a given ring of the facet spiral, to the nose tip, get merged into a common path. This applies particularly for paths emanating at the central forehead where we can clearly observe the convergence of the paths at some level of the nose profile. We draw inspiration from this observation and use a frequency histogram that accumulates the occurrences of the facets at each path. The entries of this histogram include all the facets crossed by the paths. Based on this, we propose a nose profile detection method composed of the following steps: In a first step we select a ring  $\mathcal{R}$  that passes through the forehead, which generally corresponds the last few rings, however in order to avoid border effects we choose the third ring from the last one as illustrated in (Figure 9.a). The chosen ring  $\mathcal{R}$  intersects the symmetry plane at two points within two facets located at the forehead and chin areas. We then extract a portion of the ring  $\mathcal{R}$  keeping the selected facets as the median as shown in Figure 9.b. In the third step, we generate a group of geodesic paths converging to the nose tip. These paths are represented by sequences of facets joining the two strips to the nose tip (Figure 9.c). From the two groups of facet sequences  $\mathcal{S}_1$  and  $\mathcal{S}_2$  we built two histograms that encodes the distribution of the facets across these paths (Figure 9.d). From each histogram we extract the two groups of facets having a score above a certain threshold (Figure 9.e) and in order to select the valid group of facets; we perform a 3D line fitting to the facets' vertices in each group (Figure 9.f). Finally, we choose the line producing the least residual error (Figure 9.g) to correspond to the nose profile. Figure 9.h depicts some examples of detected nose profiles.

## 6 CONCLUSIONS AND FUTURE WORK

In this work, we presented a unified framework for analyzing and describing 3D facial surface. Our representation of 3D facial surface using spiral facets has

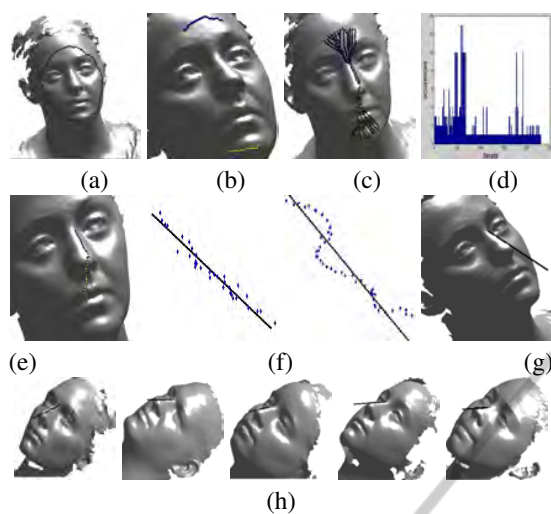


Figure 9: Nose profile detection. a: Selection of a facet rings. b: Intersection with the approximate estimation of the symmetry plane  $\Gamma$  and generation of two stripes. c: Extraction of sequences of facets following the geodesic paths from the two stripes to the nose tip. d: For each a group, a geometric histogram is computed to select facets scoring large occurrences. e: The two candidate groups of facets (in blue and yellow in colored images). f: 3D line fitting of two groups of facets and selection of the one having the lowest residual error. g: Display of the valid line passing the nose profile. h: Examples of detected nose profiles.

resulted in a mechanism that is intrinsic to the face surface, more simple, compact, generic and computationally less expensive than other popular representations. The facet spiral has wide spectrum of application that include nose tip detection, frontal face extraction, face shape description, face pose computation and nose profile identification. In the future, we plan to explore more deeply the facial shape description aspect. In this context, we plan to investigate how we can derive from the spiral curves and the concentric close curves, a kind of a "faceprint" that would uniquely define the face. We plan also to investigate further the compactness aspect of the facet spiral, the spiral-wise ordering of the facets and the topological constraints in a the facet spiral can exploited to derive a one-dimensional compressed model of the facial surface.

## REFERENCES

- Ashbrook, A. P., Fisher, R. B., Robertson, C., and Werghi, N.(1998). Finding surface correspondance for object recognition and registration using pairwise geometric histograms. In *Proc European Conference on Computer Vision*, pages 674686.
- Berretti, S., Bimbo, A. and Pala, P.(2006). Description and retrieval of 3D face models using iso-geodesic stripes. In *Conf. Multimedia Information Retrieval*, page 1322.
- Bronstein, A., Bronstein, M. and Kimmel, R.(2003). Expression invariant 3D face recognition. Audio-and Video-based Person Authentication, pages 6270.
- Chua, C., Han, F. and Ho, Y.(2000). 3D Human face recognition using point signature. In *Conf. on Automatic Face and Gesture Recognition*, pages 233238.
- Colbry, D., Stockman, G. and Jain, A.(2005). Detection of anchor points for 3D face verification. In *Proc.Computer Vision and Pattern Recognition*.
- Cormen, T. H., Leiserson, C., Rivest, R. L. and Stein., C.(2001). Introduction to Algorithms, *Second Edition*. MIT Press and McGraw-Hill.
- F. R., A.-O., Bennamoun, M. and Mian, A.(2008). Integration of local and global geometrical cues for 3D face recognition. *Pattern Recognition*, 41(3):10301040
- Frey, P. and Borouchaki, H.(1999). Surface mesh quality evaluation. *International Journal for Numerical Methods in Engineering*,45(1):101118.
- Heseltine, T., Pears, N. and Austin, J.(2008). Three-dimensional face recognition using combinations of surface feature map subspace components. *Image and Vision Computing*, 26:382-396
- Irfanoglu, M., Gokberk, B. and Akarun, L.(2004). 3D shape-based face recognition using automatically registered facial surfaces. In *Conf. Pattern Recognition*, volume4, pages 183186.
- Kakadiaris, I.(2007). Three-dimensional face recognition in the presence of facial expressions: An annotated deformable model approach. *IEEE Transaction on Pattern Analysis and Machine Intelligence*,29(4).
- Lee, Y., Park, K., Shim, J. and Yi, T.(2003). 3D face recognition using statistical multiple features for the local depth information. In *Conf. Vision Interface*, pages 102108.
- Lu, X. and Jain, A.(2005). Deformation analysis for 3D face matching. In *IEEE Workshops on Application of Computer Vision*, pages 99104.
- Mian, A., Bennamoun, M. and Owens, R.(2007). An efficient multimodal 2D-3D hybrid approach to automatic face recognition. *IEEE Transactions in Pattern Analysis and Machine Intelligence*, 29(11):19271943.
- Moreno, A., Sanchez, A. and Martinez, E.(2006). Robust representation of 3D faces for recognition. *Int. Journal of Pattern Recognition and Artificial Intelligence*, 20(8):11591186.
- Nair, P. and Cavallaro, A.(2009) 3-d face detection, landmark localization, and registration using a point distribution model. *IEEE Trans. Multimedia*, 1(4):611623.
- Pan, G., Wu, Y., Wu, Z. and Liu, W.(2003). 3D face recognition by profile and surface matching. In *IEEE/INNS Conf. on Neural Networks*, volume3, pages 21692174.
- Piegl, L. and Tiller, W.(2006) *The NURBS Book*. Springer.
- R. Niese, Al-Hamadi, A. and Michaeli, B.(2007) A novel method for 3D face detection and normalization. *Journal of Multimedia*,2(5):112.

- Romero, M. and Pears, N.(2009). Landmark localisation in 3D face data. In *IEEE Conf. on Advanced Video and Signal Based Surveillance*, pages 7378.
- Ruiz, M. and Illingworth,J.(2008). Automatic landmarking of faces in 3D-alf. In 5th International Conference on Visual Information Engineering(VIE2008), pages4146.
- Samir, C., Srivastava, A., Daoudi, M. and Klassen, E. (2009) An intrinsic framework for Analysis of facial surfaces. *International Journal of Computer Vision*, 82(1).
- Segundo, M., Queirolo, C., Bellon,O. and Silva, L.(2007). Automatic 3D facial segmentation and landmark detection. In *Proc. 14th Int.Conf. on Image Analysis and Processing*, page431436.
- Sethian, J. and Kimmel., R.(1998). Computing geodesic paths on manifolds. *Proc. National Academy of Sciences*, 95(15):84318435.
- Wang, Y., Tang, X., Liu, J., Pan, G. and Xiao, R.(2008). 3D face recognition by local shape difference boosting. In *Proc. European Conference on Computer Vision, ECCV*, pages 603616.
- Wu, Y., Pan, G. and Wu, Z.(2003). Face authentication based on multiple profiles extracted from range data. In *Conf. Audio-and Video-Based Biometric Person Authentication*, volume 2688, pages 515522.
- Xu, C., Tan, T., Wang, Y. and Quan, L.(2006) Combining local features for robust nose location in 3D facial data. *Pattern Recognition Letters*, 27:14871494.
- Xu, C., Wang, Y., Tan, T. and Quan, L.(2004a). Automatic 3D face recognition combining global geometric features with local shape variation information. In *IEEE Conf. on Automatic Face and Gesture Recognition*, pages 302307.
- Xu, C., Wang, Y., Tan, T. and Quan, L.(2004b) A new attempt to face recognition using eigenfaces. In *Asian Conference on Computer Vision*, volume 2, pages 884889.
- Xu, D., Hu, P., Cao, W. and Li, H.(2008). 3D face recognition using moment in variants. In *IEEE Int. Conference on Shape Modeling and Applications*, pages 261262.